Development of Structures for Lossless Ion Manipulations (SLIM) High Charge Capacity Array of Traps

Adam P. Huntley, Adam L. Hollerbach, Aneesh Prabhakaran, Sandilya V.B. Garimella, Cameron M. Giberson, Randolph V. Norheim, Richard D. Smith, and Yehia M. Ibrahim*

Biological Sciences Division, Pacific Northwest National Laboratory, P.O. Box 999, Richland, Washington, 99354, United States

*Corresponding Author: Yehia.ibrahim@pnnl.gov

Abstract

Enhancing the sensitivity of low abundance ions in a complex mixture without sacrificing experiment throughput is highly desirable. This work demonstrates a way to greatly improve the sensitivity of ion mobility (IM) selected ions by accumulating them in an array of high-capacity ion traps located inside a novel structures for lossless ion manipulations ion mobility spectrometer (SLIM-IMS) module. The array of ion traps used in this work consisted of seven independently controllable traps. Each trap was 386 mm long and possessed a charge capacity of ~4.5×10^8 charges, with a linear range extending to ~2.5×10^8 charges. Each ion trap could be used to extract a peak (or ions over a mobility range) from an ion mobility separation based on arrival time. Ions could be stored without losses for long times (>100 s) and then released all at once or one trap at a time. It was possible to accumulate large ion populations by extracting and storing ions over repeated IM separations. Enrichment of up to seven individual ion distributions could be performed using the seven independently controllable ion traps. Additionally, the ion trapping process effectively compressed ion populations into narrow peaks, which provides a greatly improved basis for subsequent ion manipulations. The array of high charge-capacity ion traps provides a flexible addition to SLIM and a powerful tool for IMS-MS applications requiring high sensitivity.

Keywords: charge capacity, enrichment, high resolution, ion mobility spectrometry, ion trap, mass spectrometry, SLIM, traveling waves

Introduction

Ion mobility spectrometry-mass spectrometry (IMS-MS) has been integral in the analyses of complex biological samples largely because of its sensitivity and speed compared to other analytical methods. In IMS-MS, ions of the same mass-to-charge ratio (*m/z)* but different structures can be separated through collisions with a neutral buffer gas under the influence of an electric field.[1] Common ion mobility-based approaches are field asymmetric ion mobility (FAIMS)[2], trapped ion mobility spectrometry (TIMS)[3], traveling wave ion mobility spectrometry (TWIMS)[4], and drift tube ion mobility spectrometry (DTIMS).[1, 5, 6] The ion-neutral collision cross sections (CCS) can be calculated directly from the ions' arrival time distribution (ATD) using DTIMS or indirectly through a calibration procedure (e.g., TIMS and TWIMS). In early DTIMS designs, ion gates such as the Tyndall [6] or Bradbury-Nielson design[7] were used to pulse ions from a continuous source, such as electrospray ionization (ESI), into the drift region. This pulsed ion introduction approach reduced ion utilization efficiency (percentage of ions that are utilized in the measurement) and overall sensitivity due to ions lost while the gate was closed.[8] When complex biological samples are of interest the reduction in sensitivity can be compounded by ion suppression and competition effects.[9] The impact of ion suppression can be minimized by dilution or reducing sample complexity by using, e.g., liquid chromatography (LC).[9] With little instrument modification multiplexed approaches such as Hadamard and Fourier transform IMS have been implemented to improve the utilization efficiency of gated continuous source ions.[11-13] More generally, to improve ion utilization efficiency, storage devices such as multipole ion traps and the electrodynamic ion funnel trap (IFT) have been used to collect and store source ions.[8, 14-18] Ion storage devices also had the benefit of improving the signal-to-noise (S/N) of the IMS-MS measurements because larger ion populations could be pulsed from the storage device into the IMS.[8, 15, 17] For example, Hoaglund and co-workers reported S/N improvements by factors of 10 – 30 and duty cycles of nearly 100 % when ions were stored before separation.[15] Clowers and coworkers reported improved signal intensities by up to a factor of 7 and duty cycles >50 % when ions were stored in an IFT.[8] Although storing source ions increased ion utilization efficiency and sensitivity, ions inside the storage device could be lost due to the mass discrimination effects of excessive space charge.[18-20] Space charge can affect lower *m/z* ions by changing the secular motion [19] which is observed as a reduction of the boundary *q* value.[20] To reduce spectral complexity and increase the sensitivity of low abundance species, ions were isolated and accumulated over extended times in a quadrupole ion trap.[15] Similarly, FAIMS has been used to select ions for accumulation in an ion trap,[21] which increased the utility of the trap. However, ions that are not selected for accumulation are effectively lost in these approaches.

Ion traps have also been used after an ion mobility separation for ion dissociation.[22-27] For example, mobility-selected ions have been subjected to collision-induced dissociation (CID) in linear ion traps [22, 24] and structures for lossless ion manipulations (SLIM).[25] Mobility-selected ions stored in traps have also been subjected to electron transfer dissociation (ETD) [23] and ultraviolet photon dissociation (UVPD).[22-24] In these examples, storage, enrichment and activation of mobility-selected ions have the drawback that it interferes with the separation of other ions because they must traverse ion optics sequentially. An exception to the above are SLIM traveling wave (TW) based mobility separations that can simultaneously separate and store mobility-selected ions.[25, 28] When the conditions are fixed SLIM devices can also achieve considerably higher resolutions than traditional DTIMS because ions are separated over a much longer path length.[29] Because TW voltages are low and turns that can be implemented without significant loss of ions are feasible, long serpentine paths can be used with SLIM to achieve ultrahigh resolution separations.[10, 30-36] Such serpentine paths have also been stacked to create longer physical separation paths (>40 meters).[35] Additionally, the multi-pass operation of the serpentine path provided effective path lengths that are only limited by the ion lapping phenomenon.[10]

The flexibility of electrodes laid out on a SLIM surface makes it feasible to seamlessly integrate ion manipulations such as mobility selection and storage of ions in conjunction with a mobility separation. In 2018 we presented a SLIM array of ion traps that could store mobility-selected ions.[28] The array consisted of thirty-two SLIM-based TW ion traps that were each 25.4 mm long and located near the end of a separation path. Each trap of the array was controlled simultaneously, to trap, store, and release ions. Subsequently, Rizzo and coworkers demonstrated similar SLIM-based ion traps that were used in a tandem IMS workflow to store and dissociate mobility-selected precursor ions.[25] Because SLIM-based ion traps can store mobility-selected ions without disrupting separations, low-abundant ions can be enriched by collecting them multiple times while other ions continue to separate. The accumulated ions are then sent to the mass analyzer for detection and providing broad coverage of the other sample components.

In this work, we present a new incarnation of the SLIM array of ion traps where each trap of the array is independently controlled for a better performance. The array of traps was integrated into the last level of a multilevel SLIM module.[35] The multilevel SLIM was used because of its high separation quality (compared to a single level SLIM) and optimized ion utilization because ions not selected for trapping will be detected by the mass spectrometer. The trap lengths were also increased from 25.4 mm to 386 mm to increase the charge capacity of the traps and provide a basis for repeated analysis steps or more complex manipulations. We present the charge capacity and performance metrics of the array of traps. We then illustrate how each ion trap can be independently controlled and showcase improved sensitivity

when different mobility-selected ions were accumulated in different traps over multiple collection events. Finally, we discuss the potential utility of the traps for subsequent measurements and applications.

Experimental Setup

Instrumentation and Measurements

Experiments were performed on a 3-level SLIM module integrated with an Agilent 6230B time-of-flight mass spectrometer (ToF-MS) (Figure 1).[35] The first 2 levels were used for mobility separation while the 3rd level contained an array of seven independently-controlled ion traps and a bypass. A more detailed diagram of the boards' layout is provided in the Supporting Information (Figure S1). Each trap was 386 mm long and, similar to the rest of the SLIM levels, had an electrode arrangement of 6 RF electrodes interleaved with 5 traveling wave electrodes. SLIM was operated using helium as a buffer gas at a pressure of 3.5 torr. A more detailed description of the experimental setup is provided in the Supporting Information.

The SLIM Array of Ion Traps

Each ion trap of the array was independently controlled by a state-timing sequence (STS). An example of an STS is presented with a simplified SLIM array of traps experiment diagram in Figures S2A and S2B, respectively. In this work, a typical experimental sequence consisted of four major steps: (1) ion injection, (2) TW-based mobility separation, (3) mobility-selected ion trapping, and (4) MS readout. To illustrate, the experiment STS diagram in Figure S2A shows six traces that together portray the potentials applied to a single ion trap that accumulates a population of the same ions from three separation and collection events. In this example, the stored ions are released after three collection events near the end of the third separation. The top black trace represents the injection of ions by the lowering of the CL potential in the high-pressure ion funnel. Separation was performed by first lowering the separation TW amplitude (TWs to 0-5 V_{pp}) for a selected pre-separation time (Figure 1A) and then raising the TWs amplitude (to 20-25V_{pp}) to start the mobility separation. Lowering the TW amplitude during the pre-separation allows incoming ions to accumulate inside the 2.5 m region of the first level; note that ions travel slowly through the SLIM when TWs possess low amplitudes. Ion separation occurs during the period when the green trace is high. When an ion population reaches an intersection with one of the traps (horizontal cyan-colored paths in the region marked TW_T, Figure 2B), the ions can either be directed into the trap or sent through the bypass by controlling the states of the blocking electrodes (S1-yellow trace, S2-red trace) with a solid-state switch.[37] For clarity, only the blocking electrode regions of the first trap are labeled in Figure S2B. When the state of a blocking electrode voltage is high, a static DC voltage is applied to those electrodes. When the state is low, a TW is applied. As an example, the states of the

blocking electrode regions denoted by S1 and S2 are low and high, respectively. In this configuration, ions will not be directed to the trap because of the static DC voltage applied to S2. Instead, ions will continue down along the left-hand vertical path and exit through the bypass. Alternatively, when the states of blocking electrode regions are reversed (S1 = high, S2 = low), ions are unable to continue along the green separation path because of the static DC voltage applied to S1. Instead, ions will be directed into a trap. For each separation, the duration that S1 is high and S2 is low defines the time ions are moving into the trap (i.e., the trap collection time). After mobility-selected ions have been collected, the states of S1 and S2 return to their default values. Ions inside a trap are confined between the blocking electrode regions S2 and S3 (magenta trace) by a static DC barrier applied to both sets of electrodes. The duration between the end of ion collection and subsequent release is defined as the storage time. Ions are released from a trap when the state of the S3 blocking region is low and the trap TW_T (cyan trace) is high. The release time is defined as the duration S3 is in the low state. During ion release, the TW_T amplitude increases to match that of the separation TW. This causes ions inside the trap to move to the vertical separation path on the right side and towards the exit. Ion storage times can be lengthened to allow for multiple collection events. For example, the storage time for the mobility-selected ion in Figure S2A is three times longer than a single separation because three collection events were performed before the accumulated ions were released from the trap. It is also possible to release stored ions during the same separation from which they were collected; however, ions are typically held over many separations to accumulate larger populations.

In this work, the STSs were generated using a custom-made desktop application. The state sequences were downloaded to a microcontroller, which executed changes to the array of trap switches and TWs based on the injection pulse (black trace) that signals to the microcontroller at the start of an experiment. In all cases, the separation and bypass paths possessed the same TW conditions (i.e., speed and amplitude). During the release, TW_T also possessed the same TW conditions as the separation and bypass paths. Except where noted, the amplitude of TW_T during collection and storage was 0 V.

Results and Discussion

Charge Capacity of a Trap

A Faraday charge detector was installed behind the segmented quadrupole (see Figure 1) and used to characterize the charge capacity of a single SLIM trap. Since each trap in the array is identical in design, we expected uniform performance for all traps. Singly charged leucine enkephalin ions were injected into the SLIM and then moved through the first and second levels under separation conditions before reaching the array of traps level. When the ion distributions reached the front of trap 7 (see Figure

S1C for trap designations), they were collected (S1 high, S2 low, S3 high) for a duration of 200 ms, stored (S1 low, S2, and S3 high) for 500 ms, and then released (S1 low, S2 high, S3 low). In this experiment, the collection and storage times were fixed; however, the amount of charge in the trap was varied by adjusting the ion injection time (see Figure S2A). For each injection event, ion currents were measured after ions were released from the trap. Control experiments were performed by sending mobility-separated ions through the bypass (i.e., without trapping). The amount of charge measured from the trap and bypass for each injection duration is plotted in Figure 2A. For each injection duration, the current peak area for the released ions was used to calculate the number of charges that were stored in the trap. The linear range of the trap extends to an injection duration of ~750 ms corresponding to a 'linear trap capacity' of ~2.5×10^8 charges; above this amount, the charge continued to slowly increase, and the maximum observed (~4.5×10^8 charges) compares well to a previously published value of 1.15×10^6 charges per mm in a SLIM device.[38] The trapping efficiency for up to 4.0×10^8 charges is shown in Figure 2B. Trap efficiency is defined as the number of charges measured after trapping divided by the number of charges measured after ions traversed through the bypass. As can be seen, trapping efficiency was relatively consistent for $<2.5\times10^8$ charges. However, there was a noticeable decline in trapping efficiency beyond this value. After ~4.0×10^8 charges, no more charges were detected even when injection time was increased. This data shows that the high-charge capacity traps had a linear charge capacity of up to ~2.5×10^8. For context, the ion funnel trap (IFT) has a linear range extending to ~1.5×10^7, and an Orbitrap has a charge capacity of ~10^6 charges.[8, 39]

Performance Metrics of the SLIM Array of Ion Traps

The array of traps confines ions in the axial dimension by applying blocking voltages to the entrance and exit electrodes of a trap (electrode regions S2 and S3). Ions are confined in the lateral dimension by the DC guard electrodes, and orthogonally by RF pseudopotentials. In the current design, the same guard electrodes and applied voltages are used throughout the separation and trap regions that possessed the same DC voltage. Similarly, the blocking voltage selected to direct ions to the escalators in the separation region were the same as in the trap region (S1, S2, and S3).-The following experiments were performed using the ToF mass spectrometer.

We studied how storage time affects trapping efficiency using leucine enkephalin ions. In this study, the guard and blocking voltages were 10 V and 102 V, respectively, which were optimum for ion mobility separation and ion escalator operation. Ions were collected from one separation cycle using trap 7 and stored for durations ranging from 5 – 100 seconds. Before trapping ions for each different duration, they were sent through the bypass as a reference. The signal intensities for ions released from the trap and using the bypass are plotted in Figure 3A. Figure 3B shows the trap efficiency for each storage time,

calculated as the peak area of the ions released from the trap divided by the peak area of the ions sent through the bypass. These results indicate good efficiency (80-90%) for up to 100 seconds. Most importantly, any ion losses as a function of storage time were minimal.

We then evaluated how trapping efficiency was affected when the guard and blocking voltages were varied independently. Leucine enkephalin ions were collected from one separation cycle and stored for 100 seconds. Figure S3A shows the trap efficiency (calculated as above) when the guard voltage was increased from 4 to 14 V while the blocking voltage was held at 102 V. The results showed that using a guard voltage of 10 to 12 V yielded the best trapping efficiency (~80%). Figure S3B shows the effect of blocking voltage on the trap efficiency when the guard voltage was held at 10 V. As can be seen, the blocking voltages that gave the highest trapping efficiency were between 82 and 92 V. However, it is noteworthy that using a blocking voltage of 102 V, which is the optimum voltage for the switches at the escalator regions, provided a trapping efficiency of ~73 %. The drop in efficiency due to higher voltage highlights the need to have independent control of the switches at the array of trap region to maximize efficiency.

Unlike the guard and blocking voltages, which are defined for the entire system, the TW in the trap and separation regions can be independently controlled. We evaluated the trap efficiency at different trap TW_T amplitudes (0 – 32 V_{pp}) for singly-charged tetraoctylammonium cations stored for 2 and 10 seconds (Figures S4A and S4B, respectively). The profiles for the 2 and 10-second plots were nearly identical. At higher TW amplitudes, the trap efficiency declined from 80 to 60 %. This decline is likely due to 'pushing' ions against the blocking voltage at the S3 blocking region at the end of the trap. Using lower TW amplitudes allow ions to spread throughout the entire trap volume. This data shows that using conditions that allow ions to spread easily through the trap volume will not only optimize ion trapping efficiency but will also maximize the effective ion trapping capacity.

Independent Control of Each Trap of the Array

The independent control of each trap of the SLIM array of ion traps level was first demonstrated by collecting mobiligrams of negatively charged Agilent tuning mixture ions (Figure 4) using a Faraday detector. Figure 4A shows a reference mobiligram where ions were mobility separated in the first two SLIM levels and then sent through the bypass of the array of traps level. ATDs were assigned numeric labels based on the order they were detected. The ATD peaks 1 through 9 correspond to the nine negatively charged Agilent tuning mixture ions of *m/z* 302, 602, 1034, 1334, 1634, 1934, 2234, 2534, and 2834. The ability to control the ion traps independently was demonstrated by selecting two of these ions and storing them in separate traps. The ions that correspond to peak 4 (1334 *m/z*) were directed into trap 7, and ions of peak 6 (1934 *m/z*) were directed into trap 6. All other ions were sent through the bypass.

Stored ions were released in the same order they were collected (Figure 4B) after the untrapped ions had cleared the bypass. Interestingly, when the stored ions were released, the peaks were narrower and had higher intensity than the corresponding peaks obtained without trapping. The narrow and more intense pulse of ions is an effect of ion bunching and has been observed in other trap experiments.[15, 18, 40] In our system, an ion bunching effect is caused by the TW in the trap during ion storage. The low amplitude TW tends to build the ion population near the trap exit until the ion population space charge effect becomes sufficient to push back against the TW. This highlights the role of the trap TW amplitude; that it is not set so high as to lead to ion heating or loss from the trap. We note that if the TW amplitude is set too low and ions are also introduced too quickly (i.e., a high ion current), that excessive space charge can alternatively occur at the trap entrance, and lead to ion heating or loss.

A similar demonstration of independent trap control is shown in Figure 4C where ion peaks 3 – 7 were accumulated using different traps (traps 7, 6, 5, 4, and 3 respectively) and later released in the same order. However, in this experiment, the times between the release of ions from adjacent traps were intentionally different. The effect of the varied times used in this experiment, for example, caused the adjacent ion peaks 4 and 5 to arrive more closely to each other than adjacent ion peaks 6 and 7 when they were released. The ions released from the trap in Figures 4B and 4C were detected as narrow and well-resolved peaks which also retained their relative intensities. This suggests that the ion traps could be used to compress broad peaks of low intensity, which may be otherwise difficult to quantify, into narrower peaks of higher intensity to improve quantification.

We also found it is feasible to store different ions (e.g., multiple IMS peaks) in the same trap and later release them simultaneously. Figure S5 shows mobiligrams of negatively charged Agilent tuning mixture ions acquired using the Faraday detector. Figure S5A shows the reference mobiligram (i.e., ions sent through the bypass), and the cyan box indicates the mobility range selected to send to an ion trap. In this case, the selected mobility range encompassed at least two ion peaks (*m/z* 302 and 602) and a possible contaminant. These ions were collected, stored, and released from the same trap at 2.8 s (Figure S5B). Although it has not yet been demonstrated in a SLIM device, the array of ion traps could be implemented using a dual polarity SLIM configuration [41] to enable ion-ion reactions, such as charge-reduction or dissociation.[42]

Ions collected in different traps do not need to be released in the order they were collected. Figure S6A establishes a reference mobiligram for negatively charged Agilent tune mixture ions. Figure S6B demonstrates the accumulation of 1334, 1934, and 2534 *m/z* ions and their subsequent release in the same order. In Figure S6C ions were collected in the same order as above and released as 2534, 1334, and 1934 *m/z*. Lastly, Figure S6D demonstrates the release of the ions stored in the three traps simultaneously. The

figure is zoomed in to show the ion peaks are nearly resolved. In this case, the separation primarily results from the exit path and the rear ion funnel.

Accumulation of Ions from a Complex Mixture by Successive Collection Events

In a complex mixture, some ion populations may be challenging to detect or study further (such as by MS/MS) among other highly abundant ions unless there is an initial selection or purification step. Quadrupole mass filters and ion traps, and FAIMS can be used to improve the sensitivity by filtering out other ions. However, the SLIM array of ion traps could be used to enrich the mobility-selected ions without removing or impacting the study of other ions from the sample. Here we demonstrate the accumulation of mobility-selected bovine serum albumin (BSA) tryptic digest ions over multiple separations.

A 3D heat map of a single separation of BSA digest ions is shown in Figure 5A. The area bound by the gold box emphasizes a region containing ions of moderate abundance. To demonstrate the enrichment capability of the traps, all ions in this region were accumulated for 1 to 30 separations (i.e., using 1 to 30 collection events). For this study, we focus the discussion on the enrichment of the 653 and 752 *m/z* ions (Figure 5A, circled gold). The improved sensitivities for these ions after they were accumulated are evident in Figure S7A as the enrichment ratio (the ion peak area after enrichment for *n*-collection events divided by the peak area of the ion from one collection event). Ion peak areas should increase linearly with the number of collection events assuming the ion source is stable and there is no ion loss; however, the accumulation of these ions plateaued after 10 collection events yielding a maximum enrichment ratio of approximately 10.

From the isotopic peak distributions, it is evident that the 653 and 752 *m/z* ions were doubly charged. The lower-than-anticipated enrichment ratios observed for these ions may have in part been due to charge reduction (e.g., proton transfer) due to reactions during ion storage arising from, for example, gas phase impurities or (less likely) ion activation.[43, 44] After 10 collection events, the peak areas of these doubly charged ions plateaued, and the region of the 3D heat map where stored ions were released became sensitive to the formation of new higher *m/z* ions. The signals of these higher *m/z* ions from the trap increased with the number of collection events and were most prominent after 30 events. Of the observed higher *m/z* ions, we note the formation of the singly charged 1305 and 1503 *m/z* ions (circled gold in Figure 5B) correspond to a proton loss by the 653 and 752 *m/z* ions, respectively. Figure S7B shows the areas of the 1305 and 653 *m/z* ions and their summed values. Initially, the summed area was predominantly formed by the 653 *m/z* ions. After 10 collection events, the area of the 653 *m/z* ions no longer increased; however, the 1305 *m/z* peak area continued to grow. Similarly, Figure S7C shows the formation of the 1503 *m/z* ions from the proton loss by the 752 *m/z* ions. When the areas of the charge-

reduced ions were included in the comparisons (Figure S7D) the peptide ions having initial mass-to-charge ratios of 653 and 752 *m/z* reached enrichment ratios of 25 and 20 following 30 collection events, respectively. This result indicates that charge reduction does not adversely affect the enrichment of the analyte; however, future work to assure the purity of the gas phase environment is needed to better mitigate the charge reduction during storage.

Potential Applications

In this work, we demonstrated a SLIM array of ion traps that can accumulate and enrich mobility-selected ions while simultaneously making IMS measurements of ions not selected for storage. The capabilities of these traps provide the basis and flexibility for more complex ion manipulations. The parallel operation of SLIM traps is not only useful for the enrichment of low abundant ions but could in conjunction with its spatial ion compression properties be used to facilitate post-IMS ion manipulations (e.g., CID and UVPD). For example, A SLIM ion trap could be used to accumulate different mobility-selected precursor ions which could then be subjected to UVPD or CID without disrupting the separation of other ions. Similarly, two SLIM ion traps could be used to accumulate and store the same precursor ion from different separation events; the ions of one trap could then be subjected to CID, and ions in the second trap could be subjected to UVPD. Parallel activation of ions by multiple methods could improve the throughput of certain experiments. Storage and dissociation of enriched mobility selected ions could also be implemented as a step in an IMS^n workflow. Precursor ions of the same type could be enriched and stored in separate traps. These ions could then be subjected to activation by UVPD after which fragment ions in one of the traps could be immediately mass analyzed, and ions from the other trap could undergo additional IMS separation to glean structural information. Mobility-selected fragment ions from the additional separation step could be stored and subjected to additional activation and separation. This process could be repeated numerous times if the array of traps were implemented in a cyclic SLIM.[10]

An important observation from this work is the utility of the ion accumulation and storage process that uses gentle traveling waves to essentially compress the accumulating or stored ion population (see Figures 4, S5, and S6). This compression yields higher intensity peaks that retain their relative intensities to other stored ion populations. This peak compression can effectively increase the detectability of ions, but more importantly, provide a basis for more efficient and subsequent use of select ion populations. For example, ion populations can be selected for storage in a trap to compress them into narrow and more intense peaks. These compressed ion populations can then be used for subsequent multi-pass separations in which isomers of very similar mobility are resolved.[34]

Conclusions

In this work, we presented a SLIM array of ion traps that was integrated with the multilevel SLIM.[35] The traps have a linear capacity of 2.5×10^8 charges and high storage efficiency. Each trap of the array was controlled which allowed different ions to be collected and stored together or in separate traps. We demonstrated flexibility in the order and timings of their subsequent release. The independent control of each trap of the array was then used to accumulate mobility-selected ions through a process of successive collection events (from different separations). We observed ion peak areas to linearly increase with the number of collection events. We also observed that charge reduction plays a role when ions are kept in the trap for long times highlighting the need to control gas impurities. Additionally, we described potential applications of the SLIM array of ion traps in an IMS^n workflow wherein mobility-selected ions stored together or in separate traps could be subjected to different forms of activation followed by additional separation. Finally, we note the utility of the effective ion peak compression that can be achieved by storage in the traps, and the important role of the (relatively low) TW amplitude in this region, as well as its potential utility not only for enhancing detection but also as a prelude to a subsequently targeted ultra-high-resolution IMS.

Associated Content

Supporting Information

A detailed experimental setup, a schematic layout of SLIM levels used in the current work, figures to support performance metrics, mobiligrams of negatively charged Agilent tune mix ions showing the ability of SLIM array of traps to release ion in any user-selected order, the enrichment of BSA tryptic digest mobility-selected ions through the accumulation

Notes

The authors declare no competing financial interest.

Acknowledgments

This work utilized capabilities developed under the support of the NIH National Cancer Institute (R33 CA217699) and the National Institute of General Medical Sciences (R01 GM130709-01 and P41 GM103493-15). This project was performed in the Environmental Molecular Sciences Laboratory, a DOE OBER national scientific user facility on the PNNL campus. PNNL is a multiprogram national laboratory operated by Battelle for the DOE under contract DE-AC05-76RL01830.

References

1. Burnum-Johnson, K. E.; Zheng, X.; Dodds, J. N.; Ash, J.; Fourches, D.; Nicora, C. D.; Wendler, J. P.; Metz, T. O.; Waters, K. M.; Jansson, J. K.; Smith, R. D.; Baker, E. S., Ion mobility spectrometry and the omics: Distinguishing isomers, molecular classes and contaminant ions in complex samples. *TrAC Trends in Analytical Chemistry* **2019,** *116*, 292-299.
2. Guevremont, R., High-field asymmetric waveform ion mobility spectrometry: A new tool for mass spectrometry. *Journal of Chromatography A* **2004,** *1058* (1), 3-19.
3. Michelmann, K.; Silveira, J. A.; Ridgeway, M. E.; Park, M. A., Fundamentals of Trapped Ion Mobility Spectrometry. *Journal of the American Society for Mass Spectrometry* **2015,** *26* (1), 14-24.
4. Shvartsburg, A. A.; Smith, R. D., Fundamentals of Traveling Wave Ion Mobility Spectrometry. *Analytical Chemistry* **2008,** *80* (24), 9689-9699.
5. Albritton, D. L.; Miller, T. M.; Martin, D. W.; McDaniel, E. W., Mobilities of Mass-Identified H3+ and H+ Ions in Hydrogen. *Physical Review* **1968,** *171* (1), 94-102.
6. Mason, E. A.; McDaniel, E. W., Subject Index. In *Transport Properties of Ions in Gases*, 2nd ed.; Wiley: New York: 1988.
7. Bradbury, N. E.; Nielsen, R. A., Absolute Values of the Electron Mobility in Hydrogen. *Physical Review* **1936,** *49* (5), 388-393.
8. Clowers, B. H.; Ibrahim, Y. M.; Prior, D. C.; Danielson, W. F.; Belov, M. E.; Smith, R. D., Enhanced Ion Utilization Efficiency Using an Electrodynamic Ion Funnel Trap as an Injection Mechanism for Ion Mobility Spectrometry. *Analytical Chemistry* **2008,** *80* (3), 612-623.
9. Cech, N. B.; Enke, C. G., Practical implications of some recent studies in electrospray ionization fundamentals. *Mass Spectrometry Reviews* **2001,** *20* (6), 362-387.
10. Deng, L.; Webb, I. K.; Garimella, S. V. B.; Hamid, A. M.; Zheng, X.; Norheim, R. V.; Prost, S. A.; Anderson, G. A.; Sandoval, J. A.; Baker, E. S.; Ibrahim, Y. M.; Smith, R. D., Serpentine Ultralong Path with Extended Routing (SUPER) High Resolution Traveling Wave Ion Mobility-MS using Structures for Lossless Ion Manipulations. *Analytical Chemistry* **2017,** *89* (8), 4628-4634.
11. Clowers, B. H.; Siems, W. F.; Hill, H. H.; Massick, S. M., Hadamard Transform Ion Mobility Spectrometry. *Analytical Chemistry* **2006,** *78* (1), 44-51.
12. Knorr, F. J.; Eatherton, R. L.; Siems, W. F.; Hill, H. H., Fourier Transform Ion Mobility Spectrometry. *Analytical Chemistry* **1985,** *57* (2), 402-406.
13. Chen, Y. H.; Siems, W. F.; Hill, H. H., Fourier transform electrospray ion mobility spectrometry. *Analytica Chimica Acta* **1996,** *334* (1), 75-84.
14. Henderson, S. C.; Valentine, S. J.; Counterman, A. E.; Clemmer, D. E., ESI/Ion Trap/Ion Mobility/Time-of-Flight Mass Spectrometry for Rapid and Sensitive Analysis of Biomolecular Mixtures. *Analytical Chemistry* **1999,** *71* (2), 291-301.
15. Hoaglund, C. S.; Valentine, S. J.; Clemmer, D. E., An Ion Trap Interface for ESI−Ion Mobility Experiments. *Analytical Chemistry* **1997,** *69* (20), 4156-4161.
16. Myung, S.; Lee, Y. J.; Moon, M. H.; Taraszka, J.; Sowell, R.; Koeniger, S.; Hilderbrand, A. E.; Valentine, S. J.; Cherbas, L.; Cherbas, P.; Kaufmann, T. C.; Miller, D. F.; Mechref, Y.; Novotny, M. V.; Ewing, M. A.; Sporleder, C. R.; Clemmer, D. E., Development of High-Sensitivity Ion Trap Ion Mobility Spectrometry Time-of-Flight Techniques: A High-Throughput Nano-LC-IMS-TOF Separation of Peptides Arising from a Drosophila Protein Extract. *Analytical Chemistry* **2003,** *75* (19), 5137-5145.
17. Creaser, C. S.; Benyezzar, M.; Griffiths, J. R.; Stygall, J. W., A Tandem Ion Trap/Ion Mobility Spectrometer. *Analytical Chemistry* **2000,** *72* (13), 2724-2729.
18. Ibrahim, Y. M.; Belov, M. E.; Liyu, A. V.; Smith, R. D., Automated Gain Control Ion Funnel Trap for Orthogonal Time-of-Flight Mass Spectrometry. *Analytical Chemistry* **2008,** *80* (14), 5367-5376.
19. Guo, D.; Wang, Y.; Xiong, X.; Zhang, H.; Zhang, X.; Yuan, T.; Fang, X.; Xu, W., Space Charge Induced Nonlinear Effects in Quadrupole Ion Traps. *Journal of the American Society for Mass Spectrometry* **2014,** *25* (3), 498-508.

20. Belov, M. E.; Nikolaev, E. N.; Harkewicz, R.; Masselon, C. D.; Alving, K.; Smith, R. D., Ion discrimination during ion accumulation in a quadrupole interface external to a Fourier transform ion cyclotron resonance mass spectrometer. *International Journal of Mass Spectrometry* **2001,** *208* (1), 205-225.
21. Saba, J.; Bonneil, E.; Pomiès, C.; Eng, K.; Thibault, P., Enhanced Sensitivity in Proteomics Experiments Using FAIMS Coupled with a Hybrid Linear Ion Trap/Orbitrap Mass Spectrometer. *Journal of Proteome Research* **2009,** *8* (7), 3355-3366.
22. Zucker, S. M.; Lee, S.; Webber, N.; Valentine, S. J.; Reilly, J. P.; Clemmer, D. E., An Ion Mobility/Ion Trap/Photodissociation Instrument for Characterization of Ion Structure. *Journal of the American Society for Mass Spectrometry* **2011,** *22* (9).
23. Donohoe, G. C.; Maleki, H.; Arndt, J. R.; Khakinejad, M.; Yi, J.; McBride, C.; Nurkiewicz, T. R.; Valentine, S. J., A New Ion Mobility–Linear Ion Trap Instrument for Complex Mixture Analysis. *Analytical Chemistry* **2014,** *86* (16), 8121-8128.
24. Morrison, K. A.; Clowers, B. H., Differential Fragmentation of Mobility-Selected Glycans via Ultraviolet Photodissociation and Ion Mobility-Mass Spectrometry. *Journal of the American Society for Mass Spectrometry* **2017,** *28* (6), 1236-1241.
25. Bansal, P.; Yatsyna, V.; AbiKhodr, A. H.; Warnke, S.; Ben Faleh, A.; Yalovenko, N.; Wysocki, V. H.; Rizzo, T. R., Using SLIM-Based IMS-IMS Together with Cryogenic Infrared Spectroscopy for Glycan Analysis. *Analytical Chemistry* **2020,** *92* (13), 9079-9085.
26. Bleiholder, C.; Liu, F. C.; Chai, M., Comment on Effective Temperature and Structural Rearrangement in Trapped Ion Mobility Spectrometry: TIMS Enables Native Mass Spectrometry Applications. *Analytical Chemistry* **2020**.
27. Chen, T.-C.; Ibrahim, Y. M.; Webb, I. K.; Garimella, S. V. B.; Zhang, X.; Hamid, A. M.; Deng, L.; Karnesky, W. E.; Prost, S. A.; Sandoval, J. A.; Norheim, R. V.; Anderson, G. A.; Tolmachev, A. V.; Baker, E. S.; Smith, R. D., Mobility-Selected Ion Trapping and Enrichment Using Structures for Lossless Ion Manipulations. *Analytical Chemistry* **2016,** *88* (3), 1728-1733.
28. Prabhakaran, A.; Garimella, S.; Norheim, R.; Schimelfenig, C.; Prost, S.; Giberson, C.; Ibrahim, Y.; Smith, R. In *In Implementation of Array of Traps and Ion Elevators in Structures for Lossless Ion Manipulations (SLIM)*, Proceedings of the 66th ASMS Conference on Mass Spectrometry and Allied Topics, San Diego, California, 2018.
29. Rokushika, S.; Hatano, H.; Baim, M. A.; Hill, H. H., Resolution measurement for ion mobility spectrometry. *Analytical Chemistry* **1985,** *57* (9), 1902-1907.
30. Deng, L.; Ibrahim, Y. M.; Hamid, A. M.; Garimella, S. V. B.; Webb, I. K.; Zheng, X.; Prost, S. A.; Sandoval, J. A.; Norheim, R. V.; Anderson, G. A.; Tolmachev, A. V.; Baker, E. S.; Smith, R. D., Ultra-High Resolution Ion Mobility Separations Utilizing Traveling Waves in a 13 m Serpentine Path Length Structures for Lossless Ion Manipulations Module. *Anal. Chem.* **2016,** *88* (18), 8957-8964.
31. Hamid, A. M.; Garimella, S. V. B.; Ibrahim, Y. M.; Deng, L.; Zheng, X.; Webb, I. K.; Anderson, G. A.; Prost, S. A.; Norheim, R. V.; Tolmachev, A. V.; Baker, E. S.; Smith, R. D., Achieving High Resolution Ion Mobility Separations Using Traveling Waves in Compact Multiturn Structures for Lossless Ion Manipulations. *Analytical Chemistry* **2016,** *88* (18), 8949-8956.
32. Deng, L.; Webb, I. K.; Garimella, S. V.; Hamid, A. M.; Zheng, X.; Norheim, R. V.; Prost, S. A.; Anderson, G. A.; Sandoval, J. A.; Baker, E. S.; Smith, R. D., Serpentine Ultralong Path with Extended Routing (SUPER) High Resolution Traveling Wave Ion Mobility-MS using Structures for Lossless Ion Manipulations. *Analytical Chemistry* **2017,** *89* (8), 4628-4634.
33. Ben Faleh, A.; Warnke, S.; Rizzo, T. R., Combining Ultrahigh-Resolution Ion-Mobility Spectrometry with Cryogenic Infrared Spectroscopy for the Analysis of Glycan Mixtures. *Analytical Chemistry* **2019,** *91* (7), 4876-4882.
34. Wojcik, R.; Nagy, G.; Attah, I. K.; Webb, I. K.; Garimella, S. V. B.; Weitz, K. K.; Hollerbach, A.; Monroe, M. E.; Ligare, M. R.; Nielson, F. F.; Norheim, R. V.; Renslow, R. S.; Metz, T. O.; Ibrahim, Y. M.; Smith, R. D., SLIM Ultrahigh Resolution Ion Mobility Spectrometry Separations

of Isotopologues and Isotopomers Reveal Mobility Shifts due to Mass Distribution Changes. *Anal. Chem.* **2019,** *91* (18), 11952-11962.
35. Hollerbach, A. L.; Li, A.; Prabhakaran, A.; Nagy, G.; Harrilal, C. P.; Conant, C. R.; Norheim, R. V.; Schimelfenig, C. E.; Anderson, G. A.; Garimella, S. V. B.; Smith, R. D.; Ibrahim, Y. M., Ultra-High-Resolution Ion Mobility Separations Over Extended Path Lengths and Mobility Ranges Achieved using a Multilevel Structures for Lossless Ion Manipulations Module. *Anal. Chem.* **2020,** *92* (11), 7972-7979.
36. Nagy, G.; Attah, I. K.; Conant, C. R.; Liu, W.; Garimella, S. V. B.; Gunawardena, H. P.; Shaw, J. B.; Smith, R. D.; Ibrahim, Y. M., Rapid and Simultaneous Characterization of Drug Conjugation in Heavy and Light Chains of a Monoclonal Antibody Revealed by High-Resolution Ion Mobility Separations in SLIM. *Analytical Chemistry* **2020,** *92* (7), 5004-5012.
37. Garimella, S. V. B.; Ibrahim, Y. M.; Webb, I. K.; Ipsen, A. B.; Chen, T.-C.; Tolmachev, A. V.; Baker, E. S.; Anderson, G. A.; Smith, R. D., Ion manipulations in structures for lossless ion manipulations (SLIM): computational evaluation of a 90° turn and a switch. *Analyst* **2015,** *140* (20), 6845-6852.
38. Deng, L.; Ibrahim, Y. M.; Garimella, S. V. B.; Webb, I. K.; Hamid, A. M.; Norheim, R. V.; Prost, S. A.; Sandoval, J. A.; Baker, E. S.; Smith, R. D., Greatly Increasing Trapped Ion Populations for Mobility Separations Using Traveling Waves in Structures for Lossless Ion Manipulations. *Analytical Chemistry* **2016,** *88* (20), 10143-10150.
39. Zubarev, R. A.; Makarov, A., Orbitrap Mass Spectrometry. *Analytical Chemistry* **2013,** *85* (11), 5288-5296.
40. Chen, H.; Lee, J.; Reilly, P. T. A., High-resolution ultra-high mass spectrometry: Increasing the m/z range of protein analysis. *PROTEOMICS* **2012,** *12* (19-20), 3020-3029.
41. Attah, I. K.; Nagy, G.; Garimella, S. V. B.; Norheim, R. V.; Anderson, G. A.; Ibrahim, Y. M.; Smith, R. D., Traveling-Wave-Based Electrodynamic Switch for Concurrent Dual-Polarity Ion Manipulations in Structures for Lossless Ion Manipulations. *Analytical Chemistry* **2019,** *91* (22), 14712-14718.
42. Stephenson, J. L.; McLuckey, S. A., Ion/Ion Reactions in the Gas Phase: Proton Transfer Reactions Involving Multiply-Charged Proteins. *Journal of the American Chemical Society* **1996,** *118* (31), 7390-7397.
43. Winger, B. E.; Light-Wahl, K. J.; Richard D, S., Gas-phase proton transfer reactions involving multiply charged cytochrome c ions and water under thermal conditions. *Journal of the American Society for Mass Spectrometry* **1992,** *3* (6), 624-630.
44. Iavarone, A. T.; Jurchen, J. C.; Williams, E. R., Effects of solvent on the maximum charge state and charge state distribution of protein ions produced by electrospray ionization. *Journal of the American Society for Mass Spectrometry* **2000,** *11* (11), 976-985.

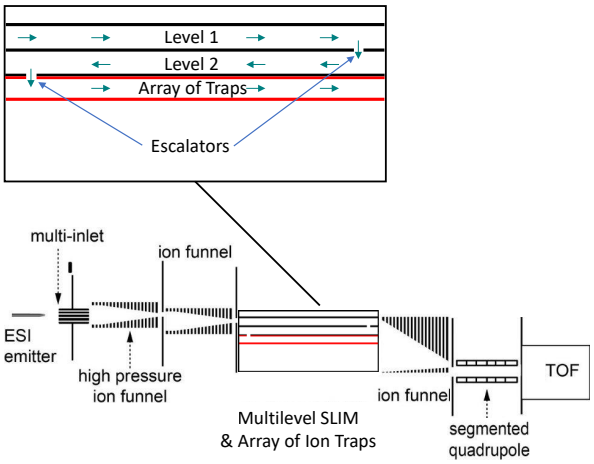

Figure 1: A schematic diagram of the multilevel SLIM and the array of traps. The cyan arrows within the inset depict the path ions take through the levels.

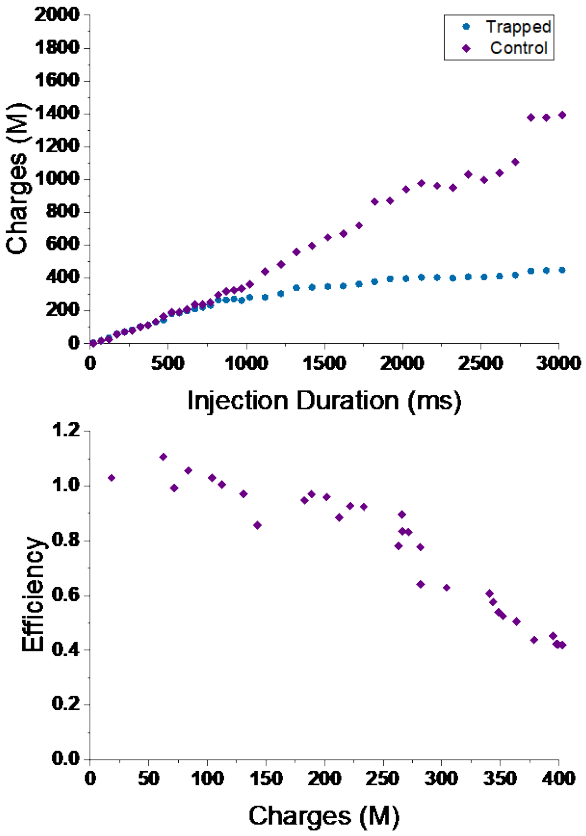

Figure 2: (A) Leucine enkephalin charges measured through the bypass (control) and after they were stored for 500 ms. (B) A plot of the efficiencies calculated from (A) for a trap to store up to 4×10^8 charges.

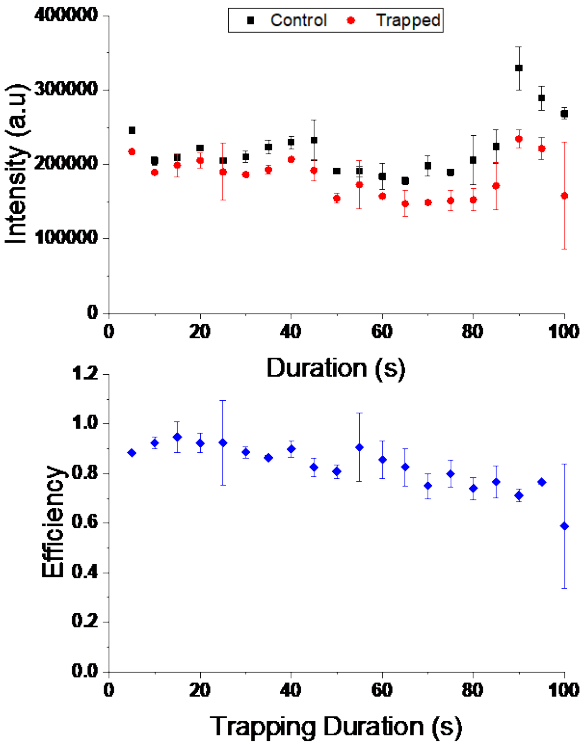

Figure 3: (A) Signal of leucine enkephalin ions through the bypass and storage durations from 5 to 100 s. (B) The trap efficiency ($I_{Trapped}/I_{Bypass}$). Guard voltage = 10 V, blocking voltage = 102 V, and TW = 0 V.

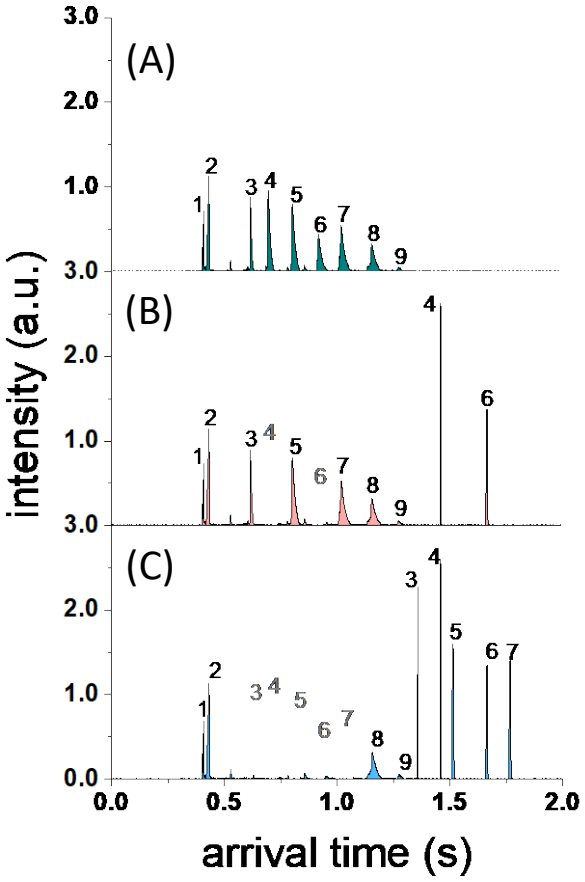

Figure 4: Mobiligrams (single unsummed) of negatively charged Agilent tune mix ions acquired with a Faraday detector. The peaks are labeled numerically in the order the ATDs were measured. (A) Reference (no trapping), (B) when peaks 4 and 6 from (A) were stored in the first and second trap nearest the bypass then released after the separation was complete, and (C) when peaks 3 – 7 from (A) were collected in the five traps nearest the bypass then released. (C) The time between the release of ions stored in adjacent traps was adjusted to affect the spacing between the pulses of released ions.

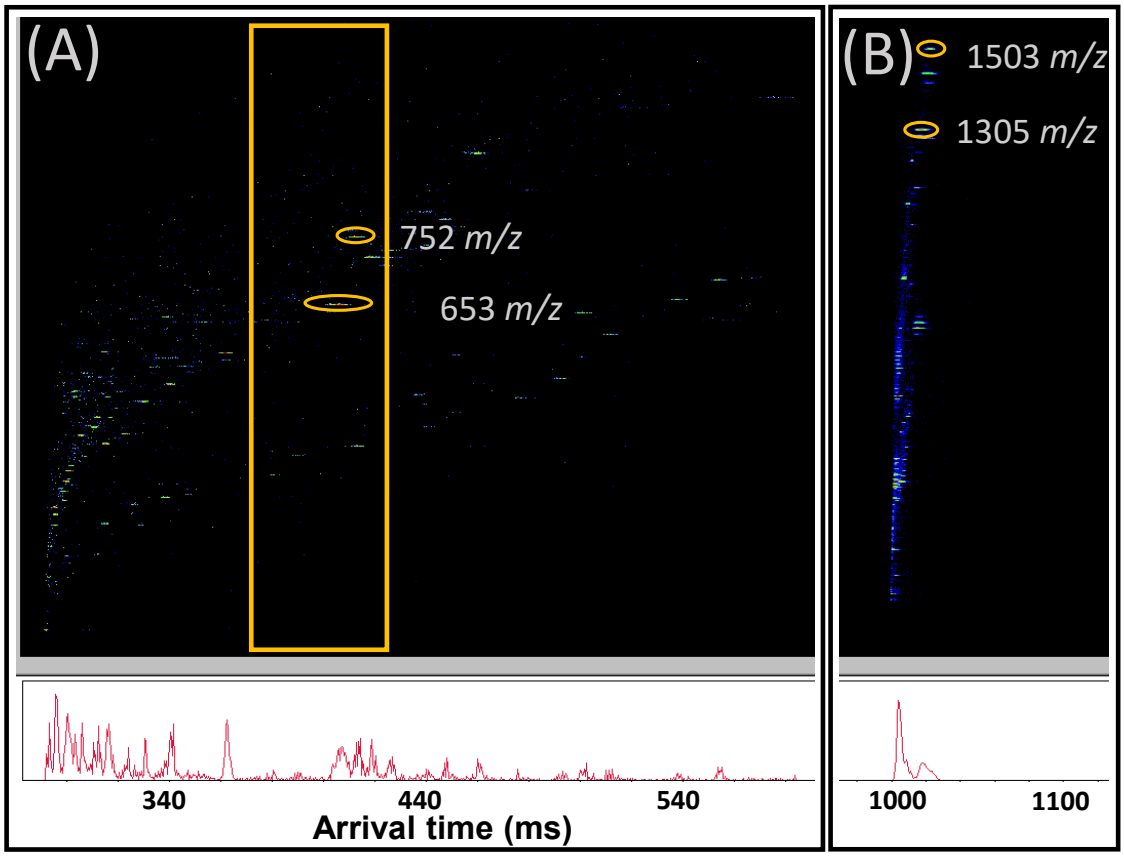

Figure 5: (A and B) 3D heat maps (unsummed) of a bovine serum albumin (BSA) digest. The gold rectangle encloses the mobility and mass range of digest peptide ions collected in trap 7 for up to 30 collection events. (A) The gold circles highlight the ions having the *m/z* of 653 and 752. (B) Release of stored ions after their accumulation over 30 collection events. The gold circles highlight the reduced charge state ions (1305 and 1503 *m/z*). The scales of A and B were truncated for figure clarity. The trap TW was set to 2 V_{PP} for all collection events.

Table of Contents Figure